Respiratory Syncytial virus NS1 protein targets the transactivator binding domain of MED25.

Running title: RSV NS1 targets MED25 ACID

Vincent Basse[a&], Jiawei Dong[b&], Andressa Peres de Oliveira[c], Pierre-Olivier Vidalain[c,d], Frederic Tangy[c], Marie Galloux[a], Jean-Francois Eleouet[a], Christina Sizun[b*], Monika Bajorek[a*]

[a]Université Paris-Saclay, INRAE, UVSQ, VIM, 78350 Jouy-en-Josas, France.

[b]Institut de Chimie des Substances Naturelles, CNRS UPR 2301, Université Paris-Saclay, 1 Avenue de la Terrasse, 91190 Gif-sur-Yvette, France.

[c] Unité de Génomique Virale et Vaccination, Institut Pasteur, CNRS UMR 3569, 75015 Paris, France.

[d] CIRI, Centre International de Recherche en Infectiologie, Univ Lyon, Inserm U1111, Université Claude Bernard Lyon 1, CNRS, UMR5308, ENS de Lyon, 69007, Lyon, France.

[*] Corresponding authors, [&] Co-first authors

ORCID:

Monika Bajorek 0000-0002-0160-4709

Christina Sizun 0000-0002-5760-2614

Abstract

Respiratory syncytial virus has evolved a unique strategy to evade host immune response by coding for two non-structural proteins NS1 and NS2. Recently it was shown that in infected cells, nuclear NS1 could be involved in transcription regulation of host genes linked to innate immune response, via an interaction with chromatin and the Mediator complex. Here we identified the MED25 Mediator subunit as an NS1 interactor in a yeast two-hybrid screen. We demonstrate that NS1 directly interacts with MED25 *in vitro* and *in cellula,* and that this interaction involves the C-terminal α3 helix of NS1 and the MED25 ACID domain. More specifically we showed by NMR that the NS1 α3 sequence primarily binds to the MED25 ACID H2 face, which is a transactivation domain (TAD) binding site for transcription regulators such as ATF6α, a master regulator of ER stress response activated upon viral infection. Moreover, we found out that the NS1 α3 helix could compete with ATF6α TAD binding to MED25. This finding points to a mechanism of NS1 interfering with innate immune response by impairing recruitment by cellular TADs of the Mediator via MED25 and hence transcription of specific genes by RNA polymerase II.

Importance

Human RSV is the leading cause of infantile bronchiolitis in the world and one of the major causes of childhood deaths in resource-poor settings. It is a major unmet target for vaccines and anti-viral drugs. RSV non-structural protein NS1 is known to antagonize the cellular immune response and was recently shown to be involved in transcription regulation of infected cells. However, the exact mechanism of this regulation is not well defined. Here we show that nuclear NS1 interacts directly with the Mediator subunit MED25 and is able to compete with a cellular transcription activator, which is activated during viral infection. We hypothesize that this interaction may underlie regulation of the expression of genes involved in the innate immune response.

Introduction

Human RSV (hRSV) is the most frequent cause of infantile bronchiolitis and pneumonia worldwide (1). In 2005 it was estimated to have caused ~34 million acute respiratory infections in children younger than 5 years and 60,000-199,000 childhood deaths worldwide (2). Severe RSV infection is a major reason for child hospitalization. The importance of RSV-associated pulmonary disease and mortality in elderly persons has also been recognized (3). Similarly, bovine RSV (bRSV) affects cattle farms and leads to economic loss due to high morbidity and mortality among calves (4, 5). Importantly, there is still no licensed vaccine for human RSV despite over six decades of attempts (6), emphasizing the need for a better understanding of RSV pathogenesis, and more particularly the mechanisms that were developed by the virus to evade host innate immune responses.

The pathology associated with RSV infection results from both viral replication and the host immune response mediated first by the production of type I interferons (IFN-I), which induces the transcription of IFN-stimulating genes (ISG) and the production of proinflammatory mediators (7, 8). However, upon infection by RSV, IFN levels remain surprisingly low. This poor induction of IFN is attributed at least in part to the two RSV non-structural proteins, NS1 and NS2. NS1 and NS2 are unique to the *Orthopneumovirus* genus of the *Pneumoviridae* family. They diverge among the different viruses of this genus and appear to contribute to host-range restrictions (5, 9, 10). Both NS1 and NS2 also act as IFN antagonists, and many of their cytosolic targets have been identified (11, 12). As an example, NS1 inhibits RIG-I activity by interacting with MAVS as well as with TRIM25, the E3 ligase of RIG-I (13, 14). NS1 and NS2 were localized to the mitochondria (15), where they form a viral degradasome, leading to degradation of multiple target proteins, notably involved in type I IFN pathway (11). NS1 was found in the cytosol as well as in the nucleus, where it is expected to interfere with host gene expression (15, 16). In a very recent publication, NS1 was shown to associate with chromatin in promotor and enhancer regions of genes related to innate immune response to viral infection (16). By targeting these DNA regulatory regions, NS1 was suggested to

suppress transcription of these genes, thus antagonizing the immune response (16). However, the exact molecular mechanism of this suppression is not well defined yet. Further study of NS1 interaction with nuclear host factors will enable a better understanding of how RSV modulates host transcription.

Based on comparison of X-ray crystallographic structures, hRSV NS1 was proposed to be a structural paralog of the hRSV matrix (M) protein (17-19). NS1 displays striking structural similarity with the N-terminal domain of the M protein, as both contain a 7-stranded β-sandwich clamped by an α-helix. In contrast to M, NS1 lacks a similar C-terminal domain but contains an additional C-terminal α-helix, α3 (Fig. 1A). NS1 α3 helix was specifically shown to be involved in the modulation of host responses (18). Mutations in the NS1 α3 helix negatively affected the transcriptional regulation of genes involved in key signalling pathways such as IFN induction and oxidative stress, resulting in 2-fold reduction of RSV replication (18).

Two different interactome studies of RSV NS1 pointed to an interaction of NS1 with the Mediator complex (16, 20). The Mediator complex is a nuclear multi-subunit complex that is part of the preinitiation complex required for RNA polymerase II transcription, and is a known regulator of many innate immune response genes (21-23). Several Mediator subunits were identified as potential interactors of NS1, among which MED25 (16, 20). MED25 was shown to be targeted by viral activator proteins, such as Herpes simplex virus transactivator protein VP16, which activates viral immediate-early genes during infection (24, 25). MED25 contains two folded domains: the N-terminal von Willebrand domain (residues 15-216, VWD) and the central Activator Interacting Domain (residues 392-543, ACID) (Fig. 1B). The interdomain and C-terminal regions are likely highly disordered. The ACID structure was solved by NMR and shown to be the target of both transactivation domains (TADs) of VP16 (24, 26, 27). A cryo-EM structure of the entire mammalian Mediator complex confirmed the location of MED25 in the tail module, with VWD well integrated in the tail (28) and ACID extending outside of the complex.

The putative interaction between NS1 and Mediator complex suggested by interactome studies has not been investigated so far. Having identified MED25 as an NS1 interactor in a yeast two-hybrid screen, we investigated this interaction in more details. We demonstrated that NS1 α3 helix directly interacts with the MED25 ACID domain in cells and *in vitro,* and that the residues found to be critical for innate immune response gene regulation (16) are also critical for this interaction. Moreover, we found out that NS1 α3 targets the MED25 ACID H2-face, which is the binding site of a number of TADs of transcription regulators (26, 27, 29-31). We revealed that NS1 α3 could compete with the TAD of ATF6α, involved in the innate immune response to viral infections. In contrast to transcription regulators like VP16, the small one-domain NS1 does not appear to have a distinct DNA-binding domain, and no specific DNA-binding region has been identified yet. Altogether, our results thus strongly suggest that NS1 could interfere with the host innate immune response by binding to MED25 and hindering the recruitment of transcription regulators to the Mediator, thus impairing transcription of specific host genes by RNA polymerase II.

Results

Identification of MED25 as a potential interaction partner of RSV NS1 by a yeast two-hybrid screen

To identify human proteins interacting with RSV NS1, we performed a yeast two-hybrid (Y2H) screen. The RSV NS1 protein fused with the GAL4 DNA binding domain (GAL4-BD) was expressed in yeast and used as a bait against prey proteins expressed from a human spleen cDNA library and fused to the GAL4 activation domain (GAL4-AD). Fifteen potential interactors of RSV NS1 were identified. We chose to focus on the MED25 subunit of the human Mediator complex, which was one of the most abundant interactors in our screen and was also identified in a previous proteomics study of host targets interacting with RSV NS1 (16, 20). In total, 10 over 156 positive yeast colonies expressed MED25. Although six of the cDNA clones expressed full-length MED25, two started at position 261 and two others at position 308. As

the four cDNA clones coding for a truncated MED25 version contained the ACID domain (Fig. 1A), this strongly suggested a role of this domain in the interaction of MED25 with RSV NS1.

NS1 interacts through its C-terminal α3 helix with MED25 ACID in cells

In order to confirm the NS1-MED25 interaction found by Y2H screening, we studied whether NS1 could interact with MED25 in cells. For that purpose, we used a split-luciferase complementation assay based on the NanoLuc enzyme (32). In this system, the 114 or the 11S NanoLuc fragments are fused to the C or N-terminus of each protein partner. To investigate the NS1-MED25 interaction, combinations of two constructs were transfected into 293T cells. Cells were lysed 24 h post transfection, luciferase substrate was added, and the luminescence, which directly depends on the interaction, was measured.

We used the RSV phosphoprotein (P), which is known to form tetramers (33-38), as a positive control. As shown in Fig. 2A, co-transfection of P-114 and P-11S resulted in a high luminescence signal, indicating a strong P/P interaction, as expected. We then used the NS1-NS1 interaction as an additional control. Although the predominant form of NS1 was reported to be monomeric (18), NS1 is also known to form dimers and higher order oligomers (15, 39). We therefore tested the NS1-114/NS1-11S pair and obtained a strong luminescence signal, revealing the capacity of NS1 to self-associate (Fig. 2A). We then tested the interaction between hRSV NS1 and full-length MED25 (Fig. 2A). When NS1-114 was co-expressed with 11S-MED25, the luminescence signal was high, confirming the interaction in cells. We then separately tested MED25 VWD and ACID domains to identify the domain involved in NS1 interaction. Transfecting NS1-114 with 11S-MED25 ACID resulted in comparable signal to that with 11S-MED25, while transfecting NS1-114 with 11S-MED25 VWD produced only background luminescence, suggesting that ACID domain was the NS1 binding domain.

We next asked whether the NS1 C-terminal α3 helix could be critical for the interaction with MED25 ACID. Previously, mutations in the α3 helix were shown to negatively affect transcription of key innate immune genes (18). We thus generated the same mutants: three NS1 mutants with substitutions inside the α3 helix, Y125A, L132A, and L132A/L133A, and a

deletion mutant Δα3, where the α3 helix was removed. Of note, the mutants Y125A and L132A/L133A were previously shown to preserve the structural integrity of NS1 (18). Luminescence was measured in cells transfected with WT or mutant NS1-114 together with 11S-MED25 ACID (Fig. 2B). NS1 L132A/MED25 ACID co-transfection resulted in luminescence signal comparable to NS1/MED25 ACID. In contrast, co-transfection of NS1 Y125A, L132A/L133A or Δα3 with MED25 ACID significantly reduced luminescence, indicating loss of interaction. All NS1 constructs were expressed in comparable amounts in cells, as assessed by Western blot using a FLAG tag (Fig. 2C). Our results with the split-NanoLuc assay thus confirmed the NS1-MED25 interaction, and allowed to identify the MED25 ACID domain and the NS1 α3 helix as interaction domains.

Last, as MED25 has been reported to localize to the nucleus (24), and since NS1 was suggested to be actively transported to the nucleus by binding another cellular or viral protein (16), we investigated whether interaction with MED25 could influence the cellular localization of NS1. BEAS-2B cells were transfected to express FLAG-NS1 WT or mutant constructs, and the localization of NS1 protein was determined by immunofluorescence imaging after staining with anti-FLAG primary antibody (Fig. 2D). Untagged NS1 was used as negative staining control. FLAG-NS1 localized to the nucleus and to the cytoplasm, as previously reported (15, 16). None of the four tested NS1 mutants showed loss of nuclear localization, indicating that the NS1-MED25 interaction is not required for NS1 nuclear localization.

NS1 interacts directly with MED25 ACID

Next, we investigated the interaction between human NS1 and MED25 ACID *in vitro* by GST-pulldowns using recombinant proteins. GST, GST-NS1 and GST-NS1α3 (residues 115-139) were co-expressed with MED25 ACID in *E.coli*. Bacteria lysates were incubated with glutathione beads, washed extensively and the bound complexes were analysed by SDS-PAGE and Coomassie blue staining. As shown in Fig. 3, MED25 ACID was pulled down by GST-NS1 as well as GST-NS1α3. Spurious binding was observed with GST without NS1. However, the relative band intensities between GST and retained MED25 ACID were

189 significantly lower than with GST-NS1 or GST-NS1α3. In conclusion, our results showed that
190 the NS1/MED25 ACID interaction is direct and mediated by the C-terminal α3 helix of NS1.

191

192 **Mapping of NS1 interaction regions on MED25 ACID by NMR**

193 To map more precisely the NS1 α3 helix interaction site on MED25 ACID, we performed NMR
194 interaction experiments. We titrated ^{15}N-labelled MED25 ACID by an N-terminally acetylated
195 peptide, NS1α3, corresponding to the sequence of the NS1 α3 helix. At each titration point we
196 acquired a 2D ^{1}H-^{15}N HSQC spectrum (Fig. 4A). The backbone chemical shifts of MED25
197 ACID were assigned *de novo* by measuring 3D triple resonance experiments on ^{13}C^{15}N-
198 labelled MED25 ACID. During the titration, perturbations of individual MED25 ACID amide
199 signals were observed, showing that the NS1α3 peptide binds to MED25 ACID (Fig. 4A). For
200 most of these residues, saturation was reached at a molar protein:peptide ratio r ~2. Due to
201 the small size of the peptide, no significant line broadening was observed for the NMR signals
202 of the complex as compared to free protein, which facilitated data analysis. Most perturbed
203 signals exhibited a linear variation of chemical shifts up to saturation, indicative of a fast
204 chemical exchange regime. Several residues, like Gly524, exhibited line broadening during
205 titration, i.e. an intermediate exchange regime between free and bound forms (inset in Fig.
206 4A). The broadened signals were recovered at r ~2. Chemical shifts perturbations (CSPs, Fig.
207 4B) at r = 1.1 were mapped onto the 3D structure of MED25 ACID (Fig. 4C). All these
208 perturbations were predominantly located on the H2 face of MED25 ACID, corresponding to
209 the binding surface of the second transactivation domain (TAD2) of VP16 (26, 27, 29).
210 Mapping of residues in intermediate exchange onto the MED25 ACID structure revealed that
211 they also belong to the H2 face (Fig. 4D), suggesting that they report on the same binding
212 event as those in fast exchange. An exchange rate between free and bound states of ~500 s^{-1}
213 was estimated from the resonance frequency difference in the intermediate exchange.
214 Intriguingly, the area perturbed by NS1α3 extends to the junction between the H1 and H2

faces, suggesting that NS1α3 binding may be accompanied by conformational rearrangement of MED25 ACID, for example by repositioning of the C-terminal α3 helix with respect to the β-barrel (Fig. 4C and 4D).

Dissociation constants (K_d) were extracted from CSPs. CSPs for residues with linear trajectories like Leu452, Met470 and Met512 were well fitted with a single binding site model (Fig. 5A-B). An average value of 17 ± 8 µM was calculated from ^{1}H and ^{15}N CSPs larger than mean+SD (Fig. 4B). The measured affinity is lower than those reported for individual TADs binding to MED25 ACID in the 0.5-1.5 µM range (26, 30, 31). However, the affinity of full-length NS1 may be higher than that of the NS1α3 peptide, since the α3 helix is preformed in NS1. We did not observe any significant H_{Ni}-H_{Ni+1} cross-peaks typical of α-helices in 2D NOESY and ROESY spectra of free NS1α3 peptide. Only residues 123-125 and 133-138, which do not display any α-helical conformation in NS1, showed weak cross-peaks, indicating that free NS1α3 peptide remains mainly unstructured.

On closer inspection, saturation was not achieved at r = 2.3 for all residues, as exemplified by Leu448 in Figure 5A. Other residues, like Ile541, displayed nonlinear chemical shift perturbation trajectories with a change at r ~1.7 (Fig. 5A). Apparent K_d values extracted from the binding curves were found in the 200 µM to 1 mM range (Fig. 5B). These results point to a second binding site of lower affinity. Mapping of the residues with high and low affinity onto the structure of MED25 ACID showed that residues with high affinity cluster on the H2 face, whereas residues with lower affinity cluster on the H1 face (Fig. 5C). Interestingly, the H1 face is the binding site for the TAD1 domain of VP16 (26, 27). Residues that sense the two binding modes cluster are located in between (Fig. 5C).

Taken together, our results show that the α3 region of NS1 primarily targets the H2 face of MED25 ACID, although weak binding also takes place at the H1 face. Even if the NS1α3 peptide is unstructured in its free form, unlike full-length NS1, it is expected to fold into an α-helix upon binding, like other TAD domains.

241

242 **NS1 competes with ATF6α for binding to MED25 ACID**

243 MED25 is a target of several transcriptional activators, from cellular and viral origin (26, 27,
244 29, 31, 40, 41), which bind either to the H1 or H2 face of MED25 ACID through their TAD
245 domains (30). While VP16TAD1 and the Ets family transcription factor ERM TAD were shown
246 to bind to H1 (27, 41), VP16TAD2 and p53TAD2 bind to H2 (26, 29, 31). Previous studies
247 have also shown that the endoplasmic reticulum stress-responsive transcription factor α
248 (ATF6α), that functions as a master regulator of ER stress response, also targets MED25 (42,
249 43), and that the TAD of ATF6α (residues 40-66, Fig. 6A) binds to the H2 site (30). Since NMR
250 results indicated that NS1 α3 helix binds to H2, we wondered whether NS1 could compete
251 with a TAD domain, by using ATF6α. A GST-ATF6α construct containing the TAD domain
252 (GST-ATF6αTAD, residues 1-150), bound to glutathione beads, was incubated with
253 recombinant MED25 ACID (30 µM) and with increasing concentrations of NS1 protein (4-32
254 µM). The bound fractions were then analysed by SDS-PAGE and Coomassie blue staining.
255 GST alone was used as a negative control. A truncated form of GST-ATF6αTAD was co-
256 purified with the full form, as shown in Fig. 6B. MED25 ACID was pulled down by GST-
257 ATF6αTAD, but not by GST (Fig. 6C), as previously published (42, 43). Adding NS1 inhibited
258 MED25 ACID binding to GST-ATF6αTAD in a dose dependent manner (Fig. 6D, upper panel).
259 SDS-PAGE analysis of the unbound fractions showed that increasing concentration of NS1
260 resulted in increasing amounts of unbound MED25 ACID (Fig. 6D lower panel). In summary,
261 these data suggest that NS1 is able to compete for MED25 ACID binding with an H2-binding
262 TAD domain such as ATF6αTAD.

263

264 **Discussion**

265 **NS1 interacts with MED25 in cells**

266 A previous proteomics study aiming to identify host partners of RSV NS1 identified several
267 proteins involved in transcription regulation, among them Mediator complex proteins (20).
268 Recent NS1 co-immunoprecipitation and mass spectrometry analysis also identified subunits

of the complex, among them MED25 (16). By using a Y2H screen, we identified MED25 as an interacting partner of NS1. Our NanoLuc interaction assay confirmed the NS1-MED25 interaction in cells and identified the MED25 ACID and NS1 C-terminal α3 helix as interaction domains (Fig. 2A and B). NS1 α3 was further confirmed by GST pull-down (Fig. 3) and by NMR (Fig. 4 and Fig. 5) to directly interact with MED25 ACID.

Interestingly, NS1 α3 helix was previously shown to contribute to the modulation of host response to RSV infection (16, 18). Mutation of residues Y125, and L132/L133 in the NS1 α3 helix or truncation of the entire α3 helix impacted the ability of NS1 to inhibit type I IFN. Moreover, recombinant RSV viruses carrying these mutations showed attenuated replication in IFN-competent cells and differential gene expression in the IFN pathways as compared to WT RSV (18). The same amino acids (Y125, L133) appeared to be critical for MED25 ACID interaction. Importantly these NS1 α3 helix point mutants can still properly localize to the nucleus (Fig. 2D), showing that the NS1-MED25 interaction is not required for NS1 nuclear transport. The structural integrity of these mutants has been verified previously (18). Strikingly, in the dimeric crystal structure of NS1, L133 and Y125 make intra-protomer and inter-protomer contacts, respectively, while L132 makes inter-and intra-protomer contacts, suggesting that they are buried in the structure and not available for interactions. If NS1 is monomeric, Y125 becomes accessible, whereas L132 and L133 anchor the α3 helix to the α,β-core of NS1. Since L133 appears to be critical for targeting MED25, this raises the question whether the α3 helix may dissociate from the α,β-core in solution.

Our NMR data indicate that the NS1α3 peptide preferentially binds to the H2 face of MED25 ACID, like several TADs of transcriptional regulators (26, 29-31). Our NMR titration experiment displayed similar features to those reported for TADs of transcription regulator VP16 and p53, i.e. similar concentrations to reach saturation and fast chemical exchange, suggesting similar binding modes and affinities. The 10-20 μM K_d obtained by NMR for NS1 α3 is indeed comparable to the 8μM value measured for the TAD2 domain of p53 by ITC (31). The 8-fold

297 molar excess of peptide needed to reach saturation in the NMR titration by VP16-H2 H2 (26)
298 also suggests 1-10 µM affinity. Surprisingly ATF6α (residues 40-66) binding, measured by
299 fluorescence anisotropy, was stronger with a K_d of 0.5 µM (30). Comparing the sequences of
300 the three H2-binding TADs with that of NS1 α3 did not reveal striking sequence similarity (Fig.
301 6A). Even residues that are critical for binding to MED25 ACID or function related to MED25
302 do not display any common pattern, apart from the requirement for hydrophobic residues (Fig.
303 6A). This is rather intriguing, but might underline that binding occurs in a multi-step process,
304 with specificities for each TAD, as already pointed out by Henderson et al (30).
305
306 **NS1 competes with cellular TADs for targeting MED25**
307 Transcription activator ATF6α functions as a master regulator of ER stress response. In
308 response to ER stress, ATF6α translocates to the Golgi, where it is processed, followed by
309 transport to the nucleus, where it activates the unfolded protein response (UPR) genes (44,
310 45). ATF6α was shown to recruit the Mediator complex by binding directly to the MED25
311 subunit (43), via the H2 site on MED25 ACID (30). Our NMR analysis showed direct binding
312 of NS1 to the MED25 ACID H2 site (Fig. 4), suggesting that NS1 might be able to compete
313 with ATF6α for binding to MED25. Our competition studies showed a decrease of MED25
314 ACID bound to ATF6α in the presence of NS1 (Fig. 6), favouring this hypothesis. Very recently
315 it was shown that RSV infection activates the UPR, partly by activating ATF6α, to enhance
316 virus production (46). While our study suggests that RSV could de-activate ATF6α by NS1
317 competing for MED25 binding, it is possible that activating and de-activating ATF6α needs to
318 be carefully balanced during RSV infection. Even as viruses utilize the host UPR to enhance
319 virus production and host cell survival, the invoked UPR in turn has the potential to sense viral
320 infection and trigger anti-viral responses (47).
321
322 Very recently, NS1 was shown to associate with chromatin, and gene regulatory elements
323 such as enhancers of genes differentially expressed during RSV infection were singled out,
324 suggesting a new role for NS1 in regulating host gene transcription (16). Importantly, 43% of

NS1 peaks identified by Chip-seq analysis coincided with Mediator peaks (16). Our results show a direct interaction between NS1 and MED25 via the H2 face of MED25 ACID, which rationalized NS1 association with Mediator peaks (16). Moreover, the Chip-seq analysis showed that the NS1 α3 helix mutant Y125A did not impact NS1 binding to chromatin, but modulated gene expression, which suggested that α3 helix may be important for interaction with a cellular partner regulating host transcription (16).

MED25 has recently emerged as one of the most significant targets for functional interactions with a range of transcriptional activators, including Herpes simplex virus transactivation protein VP16 (27, 29), ATF6α (43), ERM transcription factor (41), and p53 (31). Cellular and viral transcriptional activators that target MED25 are multi-domain proteins, which contain at least one transactivation domain (TAD) that binds the transactivator Mediator subunit MED25 and a DNA-binding domain that recognizes specific promoters/signals on target genes, which are then transcribed by RNA Pol II. Our results suggest that NS1 possesses a TAD domain and that this TAD is able to displace those of other regulation factors from the Mediator complex, thereby reducing related activation. Moreover, RSV NS1 and NS2 are the most abundantly transcribed RSV genes (15). On this basis we propose that NS1 could act as a transcription suppressor. This would present a new mechanism to control the host response upon RSV infection by interfering with activation of innate immune response genes by cellular transcriptional activators. Given the central role of NS1 in antagonizing the innate immune response to RSV, and MED25 being targetable by allosteric small molecules (30), our data could open a new avenue for RSV drug design.

MATERIALS AND METHODS

Plasmid constructs

Custom synthesized pciNanoLuc 114 and 11S vectors (GeneCust) were used to clone the codon-optimized hRSV NS1 and MED25 constructs using standard PCR, digestion and ligation techniques. pcineo NS1 single site mutants in the full-length construct were generated

353 by using the Q5 site-directed mutagenesis kit (New England BioLabs), following the
354 manufacturer recommendations. pGEX4T3 was used to clone NS1 using standard PCR,
355 digestion and ligation techniques. pGEX NS1 α3, and pGEX NS1 single site mutants were re-
356 cloned from pcineo vector using standard PCR, digestion and ligation techniques. MED25
357 (Addgene) deletion mutants were obtained by introducing start and stop codons at the
358 appropriate site in the coding sequence (MED25 VWD aa 1-231 and MED25 ACID aa 389-
359 543). pet41s GST ATF6αTAD (aa 1-150) (Addgene) contained the TAD domain.
360
361 **Y2H screen**
362 The Y2H screen was performed as previously described (48). The DNA sequence encoding
363 RSV NS1 was cloned by *in vitro* recombination (Gateway technology; Invitrogen) from
364 pDONR207 into the Y2H vector pPC97-GW to be expressed as a fusion protein with the GAL4
365 DNA-binding domain (GAL4-BD). AH109 yeast cells (Clontech; Takara, Mountain View, CA,
366 USA) were transformed with this construct using a standard lithium-acetate protocol. Screens
367 were performed on a synthetic medium lacking histidine (-His) and supplemented with 3-
368 amino-1,2,4-triazole (3-AT). A mating strategy was used to screen a commercial human
369 spleen cDNA library (Invitrogen) established in the pPC86 vector to express cellular proteins
370 in fusion downstream of the GAL4 transactivation domain (GAL4-AD). After 6 days of culture,
371 colonies were picked and replica plated over three weeks to maintain selection and eliminate
372 potential contaminants. cDNA inserts were amplified from positive yeast colonies using
373 primers that hybridize within the backbone of the pPC86 vector. After sequencing of the PCR
374 products, cellular interactors were identified by multi-parallel BLAST analysis.
375
376 **Bacteria expression and purification of recombinant proteins**
377 MED25 ACID (residues Leu389-Asn543) was produced with an N-terminal 6xHis-tag followed
378 by a T7 tag from a pET28-derived plasmid. *E. coli* BL21(DE3) bacteria transformed with the
379 pET28 MED25 ACID plasmid were grown from fresh starter culture in Luria-Bertani (LB) broth

at 37°C to an optical density of 0.6 at 600 nm, followed by induction with 0.2 mM isopropyl-β-D-thiogalactoside (IPTG) for 18 h at 20°C. Cells were lysed by sonication (4 times for 20 s each time) and lysozyme (1 mg/ml; Sigma-Aldrich) in 50 mM Na phosphate, 300 mM NaCl, 10 mM imidazole pH 8, plus protease inhibitors (Roche). Lysates were clarified by centrifugation (23,425 g, 30 min, 4°C), and the soluble MED25 ACID protein was purified on 1 ml beads loaded with Ni-NTA (GE Healthcare). The bound protein was washed extensively with loading buffer containing 25 mM imidazole and eluted with a 250 mM imidazole pH 8.

^{15}N- and $^{15}N^{13}C$-labelled MED25 ACID samples were produced in minimal M9 medium supplemented with 2 mM $MgSO_4$, 100 µM $CaCl_2$, 1X MEM vitamin solution (Gibco), 30 $\mu g \cdot mL^{-1}$ kanamycin, 1 $g \cdot L^{-1}$ $^{15}NH_4Cl$ (Eurisotop, France) and 4 $g \cdot L^{-1}$ glucose or 3 $g \cdot L^{-1}$ ^{13}C-glucose (Eurisotop, France). Expression was induced with 0.1 mM IPTG. Lysis, clarification and purification, using 2 mL Ni-NTA resin (ThermoFisher, France) per liter of culture, were carried out as described for unlabelled MED25 ACID. The eluted His-tagged protein was then dialyzed into 20 mM Na phosphate pH 6.5, 100 mM NaCl buffer supplemented with 0.5 mM dithiothreitol (DTT) using a 10 kDa cut-off membrane (Spectrapor). The protein samples were further purified by gel filtration on a Superdex S75 HR 10/30 column (GE Healthcare). Samples were then concentrated to ~500 µM using 10 kDa cut-off centrifugal filter units (Amicon Ultra, Millipore) and the DTT concentration raised to 5 mM. The concentration was determined by measuring the absorption at 280 nm and applying a molar extinction coefficient of 22,460 $mol^{-1} \cdot cm^{-1}$.

For NS1 expression, *E. coli* BL21(DE3) bacteria transformed with the pGEX-NS1 plasmid were grown from fresh starter culture in LB broth at 37°C to an optical density of 0.8 at 600 nm, followed by induction with 0.5 mM IPTG for 18 h at 20°C. Cells were lysed by sonication (4 times for 20 s each time) and lysozyme (1 mg/ml; Sigma) in 20 mM Tris-HCl, 300 mM NaCl, 5% glycerol, pH 8, plus protease inhibitors (Roche). Lysates were clarified by centrifugation (23,425 g, 30 min, 4°C), and the soluble GST-NS1 was purified on 1 ml Glutathione Sepharose beads (cytiva). The bound protein was washed with 20 mM Tris-HCl, 1M NaCl, 5% glycerol,

pH 8, followed by wash with 20 mM Tris-HCl, 300 mM NaCl, 5% glycerol, 5 mM 2-mercaptoethanol, pH 8. GST-NS1 beads were then washed with 20 mM Tris-HCl, 150 mM NaCl, 2.5 mM $CaCl_2$, 5 mM 2-mercaptoethanol, pH 8 and incubated with Biotinylated-thrombin protease (Novagen) over night at 4C. The supernatant NS1 fraction was collected and incubated with Streptavidin agarose (Millipore) for 1 h at 4°C in order to eliminate Thrombin. Purified NS1 was then concentrated using Vivaspin columns (Sartorius).

For GST and GST-ATF6αTAD expression, *E. coli* BL21(DE3) bacteria transformed with the pGEX or pet41s-ATF6α plasmid were grown from fresh starter culture in LB broth at 37°C to an optical density of 0.5 at 600 nm, followed by induction with 1 mM IPTG for 18 h at 20°C. Cells were lysed by sonication (4 times for 20 s each time) and lysozyme (1 mg/ml; Sigma) in 50 mM Tris-HCl, 300 mM NaCl, pH 8, plus protease inhibitors (Roche). Lysates were clarified by centrifugation (23,425 g, 30 min, 4°C), and the soluble GST-ATF6αTAD protein was purified on 1 ml Glutathione Sepharose beads (cytiva). The bound protein was washed extensively with 50 mM Tris-HCl and 150 mM NaCl, pH 8.

Peptide preparation

N-acetylated NS1 α3 peptide Ac-SDSTMTNYMNQLSELLGFDLNP (RSV NS1 residues Ser118-Pro139) was synthesized by GeneCust (Luxemburg) with >95% purity, as assessed by HPLC. Aliquots of 2 mg were suspended in 1 mL MQ water and dispersed by sonication. The pH was neutralized by addition of 1 M NaOH, leading to complete dissolution. The concentration was determined by measuring the absorption at 280 nm and applying a molar extinction coefficient of 1490 $mol^{-1} \cdot cm^{-1}$. The quality of the peptide solution was assessed by NMR. Aliquots were lyophilized for the titration experiment with ^{15}N-MED25 ACID.

Pull-down experiments

To validate NS1-MED25 ACID interaction, MED25 ACID was co-expressed together with GST, GST-NS1 or GST-NS1 α3 helix. *E. coli* BL21(DE3) bacteria were transformed with the

pet28 MED25 ACID plasmid together with empty pGEX, pGEX NS1, or pGEX NS1 α3 helix. Protein induction was as for MED25 ACID alone (see above). Cells were lysed by sonication (4 times for 20 s each time) and lysozyme (1 mg/ml; Sigma) in 50 mM Na Phosphate, 300 mM NaCl, pH 8, plus protease inhibitors (Roche). Lysates were clarified by centrifugation (23,425 g, 30 min, 4°C), and the soluble proteins complexes were purified on 1 ml Glutathione Sepharose beads (cytiva). Beads were washed with 50 mM Tris-HCl and 150 mM NaCl, pH 8, and the bound proteins were analysed by SDS-PAGE and Commassie staining.

Cell culture

293T cells were maintained in Dulbecco modified Eagle medium (eurobio) supplemented with 10% fetal calf serum (FCS; eurobio), 1% L-glutamine, and 1 % penicillin streptomycin. The transformed human bronchial epithelial cell line (BEAS-2B) (ATCC CRL-9609) was maintained in RPMI 1640 medium (eurobio) supplemented with 10% fetal calf serum (FCS; eurobio), 1% L-glutamine, and 1% penicillin-streptomycin. The cells were grown at 37˚C in 5% CO_2.

NS1-ATF6αTAD competition assay

GST and GST-ATF6αTAD were expressed in BL21 *E.coli* and purified on Glutathione beads as described above. 50 µl GST or GST-ATF6αTAD beads were incubated with 30 µM purified MED25 ACID without or with increasing concentration of NS1 protein (4-32µM) for 2 h at 4°C. After incubation, the supernatants were collected for analysis. Beads were washed with 50 mM Tris-HCl and 150 mM NaCl, pH 8, and the samples corresponding to proteins bound to beads or recovered in the supernatant were analysed by SDS-PAGE and Commassie staining.

NanoLuc interaction assay

Constructs expressing the NanoLuc subunits 114S and 11S were used (32). 293T cells were seeded at a concentration of $3x10^4$ cells per well in 48-well plate. After 24 h, cells were co-transfected in triplicate with 0.4 µg of total DNA (0.2 µg of each plasmid) using Lipofectamine 2000 (Invitrogen). 24 h post transfection cells were washed with PBS, and lysed for 1 h in room temperature using 50 µl NanoLuc lysis buffer (Promega). NanoLuc enzymatic activity was measured using the NanoLuc substrate (Promega). For each pair of plasmids, three normalized luminescence ratios (NLRs) were calculated as follows: the luminescence activity measured in cells transfected with the two plasmids (each viral protein fused to a different NanoLuc subunit) was divided by the sum of the luminescence activities measured in both control samples (each NanoLuc fused viral protein transfected with an plasmid expressing only the NanoLucsubunit). Data represent the mean ±SD of 4 independent experiments, each done in triplicate. Luminescence was measured using Infinite 200 Pro (Tecan, Männedorf, Switzerland).

Immunostaining and imaging

Overnight cultures of BEAS-2B cells seeded at 4 10^5 cells/well in 6-well plates (on a 16-mm micro-cover glass for immunostaining) were transfected with pcineo plasmids (0.4 µg) carrying the RSV codon-optimised NS1 or FLAG-NS1 WT or mutant constructs using Lipofectamine 2000 (Invitrogen) according to the manufacturer's recommendations. At 24 h post transfection cells were fixed with 4% paraformaldehyde in PBS for 10 min, blocked with 3% BSA in 0.2% Triton X-100–PBS for 10 min, and immunostained with monoclonal anti-FLAG (1:2000; Sigma) antibodies, followed by species-specific secondary antibody conjugated to Alexa Fluor 488 (1: 1,000; Invitrogen). Images were obtained using Nikon TE200 inverted microscope equipped with a Photometrics CoolSNAP ES2 camera. Images were processed using MetaVue software (Molecular Devices).

Nuclear Magnetic Resonance (NMR) measurements

NMR measurements were performed on a Bruker Avance III NMR spectrometer operating at a magnetic field of 18.8 T (800 MHz ^{1}H frequency) and equipped with a cryogenic TCI probe. All samples were prepared in 20 mM Na phosphate pH 6.5, 100 mM NaCl, 5 mM DTT buffer and contained 7.5 % $^{2}H_2O$ to lock the spectrometer frequency. The temperature was set to 293 K. BEST-TROSY versions of triple resonance 3D experiments (49) were acquired on $^{13}C^{15}N$-labeled MED25 ACID (460 µM final concentration) for backbone assignment, with a 0.2 ms recycling delay: HNCO, HNCA, HN(CO)CA, CB-optimized HNCACB and HN(CO)CACB. A standard 3D ^{15}N NOESY-HSQC experiment was recorded at 700 MHz on 300 µM ^{15}N-labeled MED25 ACID to confirm chemical shift assignments. ^{1}H chemical shifts were referenced to DSS. NMR data were processed within TopSpin 4.0 (Bruker Biospin, Wissembourg) and analysed with CcpNmr Analysis 2.4 software (50). The titration experiment of ^{15}N-MED25 ACID (245 µM) by NS1α3 peptide was carried out by recording 2D ^{1}H-^{15}N HSQC spectra, using a BEST-TROSY sequence. At each titration point, a lyophilized peptide aliquot was added to keep the protein concentration constant at 225 µM, starting at 0.1 and ending at 2.3 molar equivalents. Combined amide ^{1}H and ^{15}N chemical shift perturbations $\Delta\delta_{HN}$ were calculated with a scaling factor of 1/10 for ^{15}N, corresponding to the ratio of gyromagnetic ratios between ^{15}N and ^{1}H (Eq 1):

$$\Delta\delta_{\mathrm{HN}} = \sqrt{\left(\left(\delta^{1}\mathrm{H} - \delta^{1}\mathrm{H}_{ref}\right)^{2} + \left(\delta^{15}\mathrm{N} - \delta^{15}\mathrm{N}_{ref}\right)^{2}/100\right)} \qquad \text{Eq 1}$$

Dissociation constant Kd values were extracted by fitting MED25 ACID ^{1}H and/or ^{15}N chemical shift perturbations as a function of the ligand ratio, i.e. the peptide:protein molar ratio (r), with a single site binding model and assuming a fast chemical exchange regime (Eq 2), using CcpNmr Analysis software.

$$\left(\delta - \delta_{ref}\right) = \frac{1}{2}\left(\delta_{sat} - \delta_{ref}\right) \times \left(\frac{K_d}{[MED25]_{tot}} + 1 + r - \sqrt{\left(\frac{K_d}{[MED25]_{tot}} + 1 + r\right)^{2} - 4r}\right) \qquad \text{Eq 2}$$

The exchange rate between free and bound states, k_{ex}, was estimated from the resonance frequency difference Δv in the intermediate exchange according to $k_{ex} = \pi * \Delta v$.

Illustrations

Structural representations were prepared with Pymol (Schrodinger, LLC, The PyMOL Molecular Graphics System 1.3). Graphic rendering of sequence alignment was made with Espript3.0 (51).

Acknowledgements

This work was supported by Region Ile de France (DIM 1-HEALTH 2021) and Université Paris Saclay (J.D., doctoral fellowship).

Conflicts of Interest: "The authors declare no conflict of interest."

REFERENCES

1. Group TPERfCHPS. 2019. Causes of severe pneumonia requiring hospital admission in children without HIV infection from Africa and Asia:

the PERCH multi-country case-control study. Lancet 394:757-79.
2. Nair H, Nokes DJ, Gessner BD, Dherani M, Madhi SA, Singleton RJ, O'Brien KL, Roca A, Wright PF, Bruce N, Chandran A, Theodoratou E, Sutanto A, Sedyaningsih ER, Ngama M, Munywoki PK, Kartasasmita C, Simoes EA, Rudan I, Weber MW, Campbell H. 2010. Global burden of acute lower respiratory infections due to respiratory syncytial virus in young children: a systematic review and meta-analysis. Lancet 375:1545-55.
3. Coultas JA, Smyth R, Openshaw PJ. 2019. Respiratory syncytial virus (RSV): a scourge from infancy to old age. Thorax 74:986-993.
4. Easton AJ, Domachowske JB, Rosenberg HF. 2004. Animal pneumoviruses: molecular genetics and pathogenesis. Clin Microbiol Rev 17:390-412.
5. Valarcher JF, Taylor G. 2007. Bovine respiratory syncytial virus infection. Vet Res 38:153-80.
6. Openshaw PJM, Chiu C, Culley FJ, Johansson C. 2017. Protective and Harmful Immunity to RSV Infection. Annu Rev Immunol 35:501-532.
7. Russell CD, Unger SA, Walton M, Schwarze J. 2017. The Human Immune Response to Respiratory Syncytial Virus Infection. Clin Microbiol Rev 30:481-502.
8. Hijano DR, Vu LD, Kauvar LM, Tripp RA, Polack FP, Cormier SA. 2019. Role of Type I Interferon (IFN) in the Respiratory Syncytial Virus (RSV) Immune Response and Disease Severity. Front Immunol 10:566.
9. Bossert B, Conzelmann KK. 2002. Respiratory syncytial virus (RSV) nonstructural (NS) proteins as host range determinants: a chimeric bovine RSV with NS genes from human RSV is attenuated in interferon-competent bovine cells. J Virol 76:4287-93.

10. Collins PL, Karron, R.A. 2013. Respiratory syncytial virus and metapneumovirus. *In* Wolters K (ed), Chapter in Fields of Virology, Sixt edition, vol 1.
11. Thornhill EM, Verhoeven D. 2020. Respiratory Syncytial Virus's Non-structural Proteins: Masters of Interference. Front Cell Infect Microbiol 10:225.
12. Sedeyn K, Schepens B, Saelens X. 2019. Respiratory syncytial virus nonstructural proteins 1 and 2: Exceptional disrupters of innate immune responses. PLoS Pathog 15:e1007984.
13. Boyapalle S, Wong T, Garay J, Teng M, San Juan-Vergara H, Mohapatra S. 2012. Respiratory syncytial virus NS1 protein colocalizes with mitochondrial antiviral signaling protein MAVS following infection. PLoS One 7:e29386.
14. Ban J, Lee NR, Lee NJ, Lee JK, Quan FS, Inn KS. 2018. Human Respiratory Syncytial Virus NS 1 Targets TRIM25 to Suppress RIG-I Ubiquitination and Subsequent RIG-I-Mediated Antiviral Signaling. Viruses 10.
15. Swedan S, Andrews J, Majumdar T, Musiyenko A, Barik S. 2011. Multiple functional domains and complexes of the two nonstructural proteins of human respiratory syncytial virus contribute to interferon suppression and cellular location. J Virol doi:10.1128/JVI.00413-11.
16. Pei J, Beri NR, Zou AJ, Hubel P, Dorando HK, Bergant V, Andrews RD, Pan J, Andrews JM, Sheehan KCF, Pichlmair A, Amarasinghe GK, Brody SL, Payton JE, Leung DW. 2021. Nuclear-localized human respiratory syncytial virus NS1 protein modulates host gene transcription. Cell Rep 37:109803.
17. Money VA, McPhee HK, Mosely JA, Sanderson JM, Yeo RP. 2009. Surface features of a Mononegavirales matrix protein indicate sites of membrane interaction. Proc Natl Acad Sci U S A 106:4441-6.
18. Chatterjee S, Luthra P, Esaulova E, Agapov E, Yen BC, Borek DM, Edwards MR, Mittal A, Jordan DS, Ramanan P, Moore ML, Pappu RV, Holtzman MJ, Artyomov MN, Basler CF, Amarasinghe GK, Leung DW. 2017. Structural basis for human respiratory syncytial virus NS1-mediated modulation of host responses. Nat Microbiol 2:17101.
19. Forster A, Maertens GN, Farrell PJ, Bajorek M. 2015. Dimerization of matrix protein is required for budding of respiratory syncytial virus. J Virol 89:4624-35.
20. Wu W, Tran KC, Teng MN, Heesom KJ, Matthews DA, Barr JN, Hiscox JA. 2012. The interactome of the human respiratory syncytial virus NS1 protein highlights multiple effects on host cell biology. J Virol 86:7777-89.
21. Flanagan PM, Kelleher RJ, 3rd, Sayre MH, Tschochner H, Kornberg RD. 1991. A mediator required for activation of RNA polymerase II transcription in vitro. Nature 350:436-8.
22. Kim YJ, Bjorklund S, Li Y, Sayre MH, Kornberg RD. 1994. A multiprotein mediator of transcriptional activation and its interaction with the C-terminal repeat domain of RNA polymerase II. Cell 77:599-608.
23. Soutourina J. 2018. Transcription regulation by the Mediator complex. Nat Rev Mol Cell Biol 19:262-274.
24. Mittler G, Stuhler T, Santolin L, Uhlmann T, Kremmer E, Lottspeich F, Berti L, Meisterernst M. 2003. A novel docking site on Mediator is critical for activation by VP16 in mammalian cells. EMBO J 22:6494-504.
25. Yang F, DeBeaumont R, Zhou S, Naar AM. 2004. The activator-recruited cofactor/Mediator coactivator subunit ARC92 is a functionally important target of the VP16 transcriptional activator. Proc Natl Acad Sci U S A 101:2339-44.
26. Vojnic E, Mourao A, Seizl M, Simon B, Wenzeck L, Lariviere L, Baumli S, Baumgart K, Meisterernst M, Sattler M, Cramer P. 2011. Structure and VP16 binding of the Mediator Med25 activator interaction domain. Nat Struct Mol Biol 18:404-9.
27. Milbradt AG, Kulkarni M, Yi T, Takeuchi K, Sun ZY, Luna RE, Selenko P, Naar AM, Wagner G. 2011. Structure of the VP16 transactivator target in the Mediator. Nat Struct Mol Biol 18:410-5.

598 28. Zhao H, Young N, Kalchschmidt J, Lieberman J, El Khattabi L, Casellas R, Asturias FJ. 2021.
599 Structure of mammalian Mediator complex reveals Tail module architecture and interaction
600 with a conserved core. Nat Commun 12:1355.
601 29. Bontems F, Verger A, Dewitte F, Lens Z, Baert JL, Ferreira E, de Launoit Y, Sizun C, Guittet E,
602 Villeret V, Monte D. 2011. NMR structure of the human Mediator MED25 ACID domain. J
603 Struct Biol 174:245-51.
604 30. Henderson AR, Henley MJ, Foster NJ, Peiffer AL, Beyersdorf MS, Stanford KD, Sturlis SM,
605 Linhares BM, Hill ZB, Wells JA, Cierpicki T, Brooks CL, 3rd, Fierke CA, Mapp AK. 2018.
606 Conservation of coactivator engagement mechanism enables small-molecule allosteric
607 modulators. Proc Natl Acad Sci U S A 115:8960-8965.
608 31. Lee MS, Lim K, Lee MK, Chi SW. 2018. Structural Basis for the Interaction between p53
609 Transactivation Domain and the Mediator Subunit MED25. Molecules 23.
610 32. Dixon AS, Schwinn MK, Hall MP, Zimmerman K, Otto P, Lubben TH, Butler BL, Binkowski BF,
611 Machleidt T, Kirkland TA, Wood MG, Eggers CT, Encell LP, Wood KV. 2016. NanoLuc
612 Complementation Reporter Optimized for Accurate Measurement of Protein Interactions in
613 Cells. ACS Chem Biol 11:400-8.
614 33. Castagne N, Barbier A, Bernard J, Rezaei H, Huet JC, Henry C, Da Costa B, Eleouet JF. 2004.
615 Biochemical characterization of the respiratory syncytial virus P-P and P-N protein complexes
616 and localization of the P protein oligomerization domain. J Gen Virol 85:1643-53.
617 34. Llorente MT, Taylor IA, Lopez-Vinas E, Gomez-Puertas P, Calder LJ, Garcia-Barreno B, Melero
618 JA. 2008. Structural properties of the human respiratory syncytial virus P protein: evidence for
619 an elongated homotetrameric molecule that is the smallest orthologue within the family of
620 paramyxovirus polymerase cofactors. Proteins 72:946-58.
621 35. Gilman MSA, Liu C, Fung A, Behera I, Jordan P, Rigaux P, Ysebaert N, Tcherniuk S, Sourimant J,
622 Eleouet JF, Sutto-Ortiz P, Decroly E, Roymans D, Jin Z, McLellan JS. 2019. Structure of the
623 Respiratory Syncytial Virus Polymerase Complex. Cell 179:193-204 e14.
624 36. Simabuco FM, Asara JM, Guerrero MC, Libermann TA, Zerbini LF, Ventura AM. 2011. Structural
625 analysis of human respiratory syncytial virus p protein: identification of intrinsically disordered
626 domains. Braz J Microbiol 42:340-5.
627 37. Noval MG, Esperante SA, Molina IG, Chemes LB, Prat-Gay G. 2016. Intrinsic Disorder to Order
628 Transitions in the Scaffold Phosphoprotein P from the Respiratory Syncytial Virus RNA
629 Polymerase Complex. Biochemistry 55:1441-54.
630 38. Pereira N, Cardone C, Lassoued S, Galloux M, Fix J, Assrir N, Lescop E, Bontems F, Eleouet JF,
631 Sizun C. 2017. New Insights into Structural Disorder in Human Respiratory Syncytial Virus
632 Phosphoprotein and Implications for Binding of Protein Partners. J Biol Chem 292:2120-2131.
633 39. Pretel E, Sanchez IE, Fassolari M, Chemes LB, de Prat-Gay G. 2015. Conformational
634 Heterogeneity Determined by Folding and Oligomer Assembly Routes of the Interferon
635 Response Inhibitor NS1 Protein, Unique to Human Respiratory Syncytial Virus. Biochemistry
636 54:5136-46.
637 40. Yang M, Hay J, Ruyechan WT. 2008. Varicella-zoster virus IE62 protein utilizes the human
638 mediator complex in promoter activation. J Virol 82:12154-63.
639 41. Landrieu I, Verger A, Baert JL, Rucktooa P, Cantrelle FX, Dewitte F, Ferreira E, Lens Z, Villeret
640 V, Monte D. 2015. Characterization of ERM transactivation domain binding to the ACID/PTOV
641 domain of the Mediator subunit MED25. Nucleic Acids Res 43:7110-21.
642 42. Sela D, Chen L, Martin-Brown S, Washburn MP, Florens L, Conaway JW, Conaway RC. 2012.
643 Endoplasmic reticulum stress-responsive transcription factor ATF6alpha directs recruitment
644 of the Mediator of RNA polymerase II transcription and multiple histone acetyltransferase
645 complexes. J Biol Chem 287:23035-45.
646 43. Sela D, Conkright JJ, Chen L, Gilmore J, Washburn MP, Florens L, Conaway RC, Conaway JW.
647 2013. Role for human mediator subunit MED25 in recruitment of mediator to promoters by

endoplasmic reticulum stress-responsive transcription factor ATF6alpha. J Biol Chem 288:26179-26187.

44. Haze K, Yoshida H, Yanagi H, Yura T, Mori K. 1999. Mammalian transcription factor ATF6 is synthesized as a transmembrane protein and activated by proteolysis in response to endoplasmic reticulum stress. Mol Biol Cell 10:3787-99.

45. Chen X, Shen J, Prywes R. 2002. The luminal domain of ATF6 senses endoplasmic reticulum (ER) stress and causes translocation of ATF6 from the ER to the Golgi. J Biol Chem 277:13045-52.

46. Qiao D, Skibba M, Xu X, Garofalo RP, Zhao Y, Brasier AR. 2021. Paramyxovirus replication induces the Hexosamine Biosynthetic Pathway and Mesenchymal Transition via the IRE1a-XBP1s arm of the Unfolded Protein Response. Am J Physiol Lung Cell Mol Physiol doi:10.1152/ajplung.00127.2021.

47. Smith JA. 2014. A new paradigm: innate immune sensing of viruses via the unfolded protein response. Front Microbiol 5:222.

48. Vidalain PO, Jacob Y, Hagemeijer MC, Jones LM, Neveu G, Roussarie JP, Rottier PJ, Tangy F, de Haan CA. 2015. A field-proven yeast two-hybrid protocol used to identify coronavirus-host protein-protein interactions. Methods Mol Biol 1282:213-29.

49. Solyom Z, Schwarten M, Geist L, Konrat R, Willbold D, Brutscher B. 2013. BEST-TROSY experiments for time-efficient sequential resonance assignment of large disordered proteins. J Biomol NMR 55:311-21.

50. Vranken WF, Boucher W, Stevens TJ, Fogh RH, Pajon A, Llinas M, Ulrich EL, Markley JL, Ionides J, Laue ED. 2005. The CCPN data model for NMR spectroscopy: development of a software pipeline. Proteins 59:687-96.

51. Gouet P, Robert X, Courcelle E. 2003. ESPript/ENDscript: Extracting and rendering sequence and 3D information from atomic structures of proteins. Nucleic Acids Res 31:3320-3.

FIGURE LEGENDS

Figure 1: Representation of hRSV NS1 and MED25 structural organisation. (A) Structural organization of hRSV NS1 protein, which displays an α,β-core domain and a C-terminal α3 helix. Sequence alignment of *Orthopneumovirus* NS1 proteins: hRSV NS1 construct used in the present study, human RSV A (Uniprot P0DOE9), B (O42083) and Long (Q86306) strains, bovine RSV (Q65694) and ovine RSV (Q65703). Alignment was generated on the ClustalW server. The secondary structure elements observed in the crystallographic structure of hRSV NS1 (18) are indicated above the sequence. **(B)** Domain architecture of the Mediator subunit MED25 that contains two folded domains: the N-terminal von Willebrand domain (VWD) and the central activator interaction domain (ACID) (26, 27). The boundaries of the constructs used in this study are indicated.

686 **Figure 2: NS1 interacts with MED25 in cells.** MED25 and NS1 interactions were measured
687 using the NanoLuc assay **(A)** using MED25 domain deletions or **(B)** using MED25 ACID and
688 FLAG NS1 WT and α3 helix mutants. 293T cells were transfected with pairs of constructs,
689 combined as shown in the graph. P/P and NS1/NS1 were used as positive controls. The NLR
690 is the ratio between actual read and negative controls (each protein with the empty NanoLUC
691 vector). The graph is representative of four independent experiments, each done in three
692 technical repeats. Data represents the means and error bars represent standard deviation
693 across 4 independent biological replicates. *p<0.05, **p<0.01, ***p<0.001 (unpaired two-tailed
694 t-test). **(C)** 293T cells were transfected with plasmids encoding NS1, FLAG NS1 or FLAG NS1
695 mutants fused to 114 NanoLUC subunit, and cell lysates were then subjected to Western
696 analysis using anti-FLAG antibody. Size markers are shown on the left side of the gel. **(D)**
697 BEAS-2B cells were transfected with plasmids encoding NS1, FLAG NS1 or FLAG NS1
698 mutants fused to 114 NanoLUC subunit. Cells were fixed, and immunostained with anti-FLAG
699 (green) antibody followed by Alexa Fluor secondary antibody, and were analysed by
700 microscopy**.** Scale bars represent 10µm.

701 **Figure 3: Validation of NS1-MED25 ACID interaction by GST pull-down assay. (A)**
702 MED25 ACID was co-expressed together with GST, GST-NS1, GST-NS1 α3 helix in *E. coli*
703 BL21(DE3) bacteria. Bacteria lysates were clarified and the soluble proteins complexes were
704 purified on glutathione-Sepharose beads. After extensive washing the binding of MED25 ACID
705 to GST, GST-NS1 and GST-NS1 α3 helix was analysed by SDS-PAGE and Coomassie bleu
706 staining. **(B)** Band intensities were quantified with J imager.
707
708 **Figure 4: Interaction of NS1 α3 peptide with MED25 ACID followed by NMR. (A)** Overlay
709 of 2D ^{1}H-^{15}N HSQC spectra acquired during a titration of 225 µM ^{15}N-labeled MED25 ACID
710 with increasing amounts of NS1 α3 peptide. The reference spectrum without peptide is shown
711 in red. The titration endpoint at a peptide:protein molar ratio r = 2.3 is in medium blue.
712 Intermediate titration points at r = 0.1, 0.2, 0.4, 0.6, 0.85, 1.1, 1.4, and 1.7 are colour coded

from dark orange to dark blue. Arrows show the titration direction. **(B)** Combined ^{1}H and ^{15}N amide chemical shift perturbations ($\Delta\delta_{HN}$) are stack plotted as a function of the residue number in the MED25 ACID construct for r = 1.1 (black bars) and r = 2.3 (empty bars). The bars at r = 2.3 were cut for residues Thr460 and Leu513 ($\Delta\delta_{HN}$ > 0.3 ppm). The mean value and mean plus one and two standard deviations (SD) for r = 1.1 are indicated by broken lines. **(C)** Chemical shift perturbations at r = 1.1 are mapped onto the structure of MED25 ACID (pdb 2xnf). Amide nitrogen atoms are drawn as spheres in green for residues with $\Delta\delta_{HN}$ ≥ mean+2×SD and in yellow when $\Delta\delta_{HN}$ ≥ mean+SD. The two views, corresponding to the H2 and H1 faces of MED25 ACID, are rotated by 180°. **(D)** Several signals are broadened at intermediate titration points due to an intermediate exchange regime, as exemplified by Gly524 in the inset shown on the ^{1}H-^{15}N HSQC spectra in (A). Residues in intermediate exchange regime are highlighted in orange.

Figure 5: Binding modes of NS1 α3 peptide to H1 and H2 faces of MED25 ACID. (A) Three types of chemical shift perturbation trajectories, shown for selected residues, were observed during the ^{1}H-^{15}N HSQC titration of ^{15}N-MED25 ACID by the NS1 α3 peptide. Arrows show the titration direction. The colour is varied from red to medium blue for molar peptide:protein ratios r = 0 to 2.3, with titration points at r = 0.1, 0.2, 0.3, 0.4, 0.6, 0.85, 1.1, 1.4, and 1.7. (B) The ^{15}N or ^{1}H chemical shift dimensions of the titration curves, shown in A, were fitted with a single binding site model, assuming fast chemical exchange. Experimental points are represented with solid symbols and the fitted curve in broken lines. The apparent dissociation constants K_d obtained from each fit are indicated. **(C)** Residues with high chemical shift perturbations are mapped onto the structure of MED25 ACID (pdb 2xnf) by representing their amide nitrogen in a sphere colour coded according to their binding mode. Residues with higher affinity, i.e. with apparent K_d values ranging from 7-40 µM, are indicated in red. Residues with high chemical shift perturbations, but for which saturation was not achieved at r = 2.3 are shown in blue. Residues that report on both binding events are represented in magenta. The three views are rotated by 90°.

Figure 6: NS1 competes with ATF6α for binding to MED25. (A) Sequence alignment of NS1 α3 with transactivator domains of transcription factors p53, VP16 and ATF6α. The letter Φ indicates hydrophobic or aromatic amino acids. Bold letters indicate residues that form an α-helix either in the unbound state or when bound to MED25 ACID (18, 26, 31, 43). Underlined letters indicate residues that are critical for the interaction of NS1 α3, p53TAD2 and ATF6α with MED25 ACID or critical for transcription in yeast for VP16H2. **(B)** SDS-PAGE and Coomassie blue staining of purified recombinant GST, GST- ATF6αTAD, MED25 ACID and NS1 protein. **(C)** GST or GST-ATF6αTAD were expressed in *E. coli* BL21(DE3), purified on glutathione-Sepharose beads, and incubated in the presence of MED25 ACID. After extensive washing the binding of MED25 ACID to GST and GST-ATF6αTAD was determined by SDS-PAGE and Coomassie bleu staining. **(D)** GST-ATF6αTAD protein was purified on glutathione-Sepharose beads and incubated in the presence of MED25 ACID (30μM) or MED25 ACID with increasing concentration of NS1 as indicated. After incubation supernatants were collected; beads were extensively washed and the binding of MED25 ACID to ATF6αTAD and the proteins in the supernatants were analysed by SDS-PAGE and Coomassie blue staining (upper and lower gels respectively).

Fig. 1

A

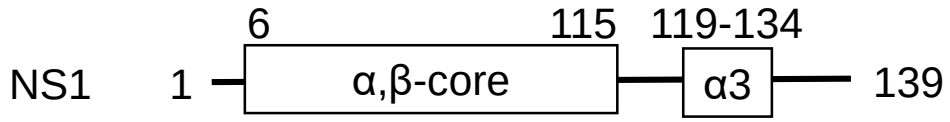
6
115
119-134
NS1
1
α,β-core
α3
139

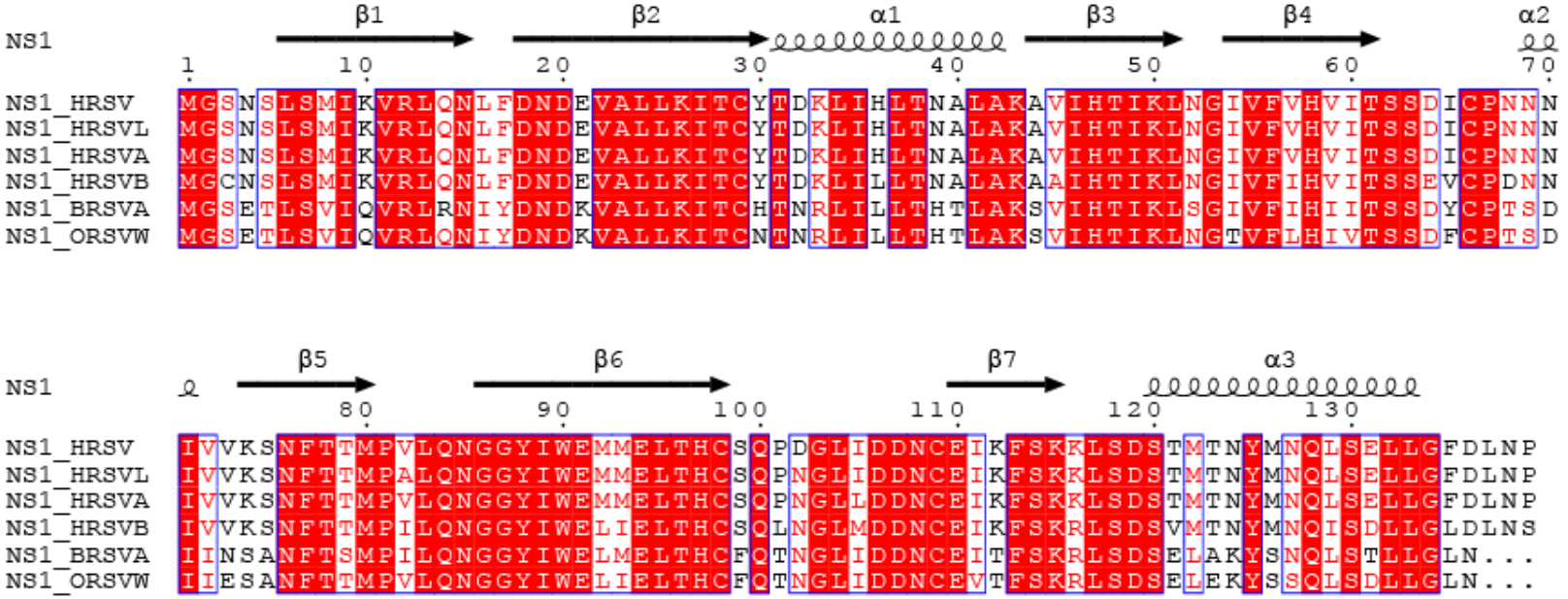
β1
β2
α1
β3
β4
α2
NS1
1
10
20
30
40
50
60
70
NS1_HRSV MGSNSLSMIKVRLQNLFDNDEVALLKITCYTDKLIHLTNALAKAVIHTIKLNGIVFVHVITSSDICPNNN
NS1_HRSVL MGSNSLSMIKVRLQNLFDNDEVALLKITCYTDKLIHLTNALAKAVIHTIKLNGIVFVHVITSSDICPNNN
NS1_HRSVA MGSNSLSMIKVRLQNLFDNDEVALLKITCYTDKLIHLTNALAKAVIHTIKLNGIVFVHVITSSDICPNNN
NS1_HRSVB MGCNSLSMIKVRLQNLFDNDEVALLKITCYTDKLILLTNALAKAAIHTIKLNGIVFIHVITSSEVCPDNN
NS1_BRSVA MGSETLSVIQVRLRNIYDNDKVALLKITCHTNRLILLTHTLAKSVIHTIKLSGIVFIHIITSSDYCPTSD
NS1_ORSVW MGSETLSVIQVRLQNIYDNDKVALLKITCNTNRLILLTHTLAKSVIHTIKLNGTVFLHIVTSSDFCPTSD
β5
β6
β7
α3
NS1
80
90
100
110
120
130
NS1_HRSV IVVKSNFTTMPVLQNGGYIWEMMELTHCSQPDGLIDDNCEIKFSKKLSDSTMTNYMNQLSELLGFDLNP
NS1_HRSVL IVVKSNFTTMPALQNGGYIWEMMELTHCSQPNGLIDDNCEIKFSKKLSDSTMTNYMNQLSELLGFDLNP
NS1_HRSVA IVVKSNFTTMPVLQNGGYIWEMMELTHCSQPNGLLDDNCEIKFSKKLSDSTMTNYMNQLSELLGFDLNP
NS1_HRSVB IVVKSNFTTMPILQNGGYIWELIELTHCSQLNGLMDDNCEIKFSKRLSDSVMTNYMNQISDLLGLDLNS
NS1_BRSVA IINSANFTSMPILQNGGYIWELMELTHCFQTNGLIDDNCEITFSKRLSDSELAKYSNQLSTLLGLN...
NS1_ORSVW IIESANFTTMPVLQNGGYIWELIELTHCFQTNGLIDDNCEVTFSKRLSDSELEKYSSQLSDLLGLN...

B

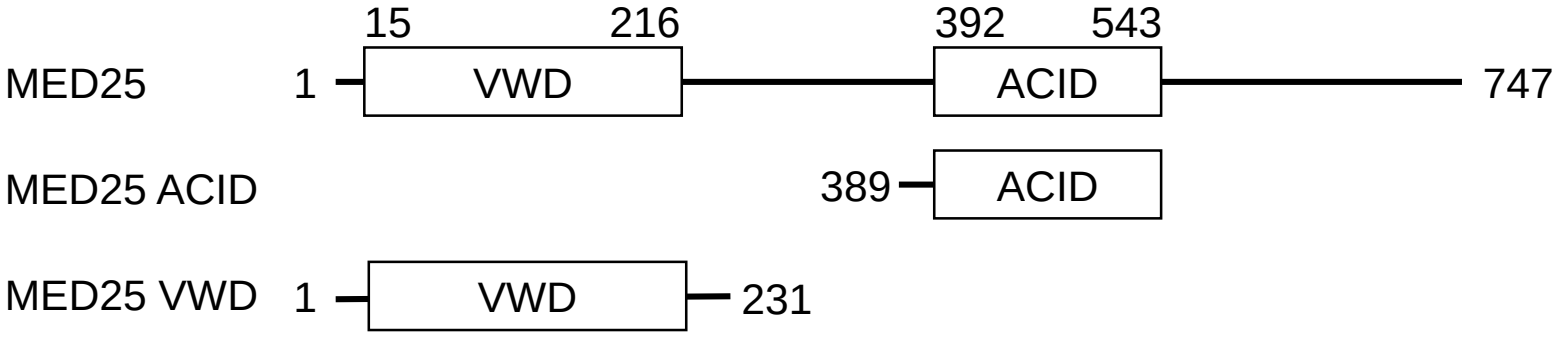
15
216
392
543
MED25
1
VWD
ACID
747
MED25 ACID
389
ACID
MED25 VWD
1
VWD
231

Fig. 2

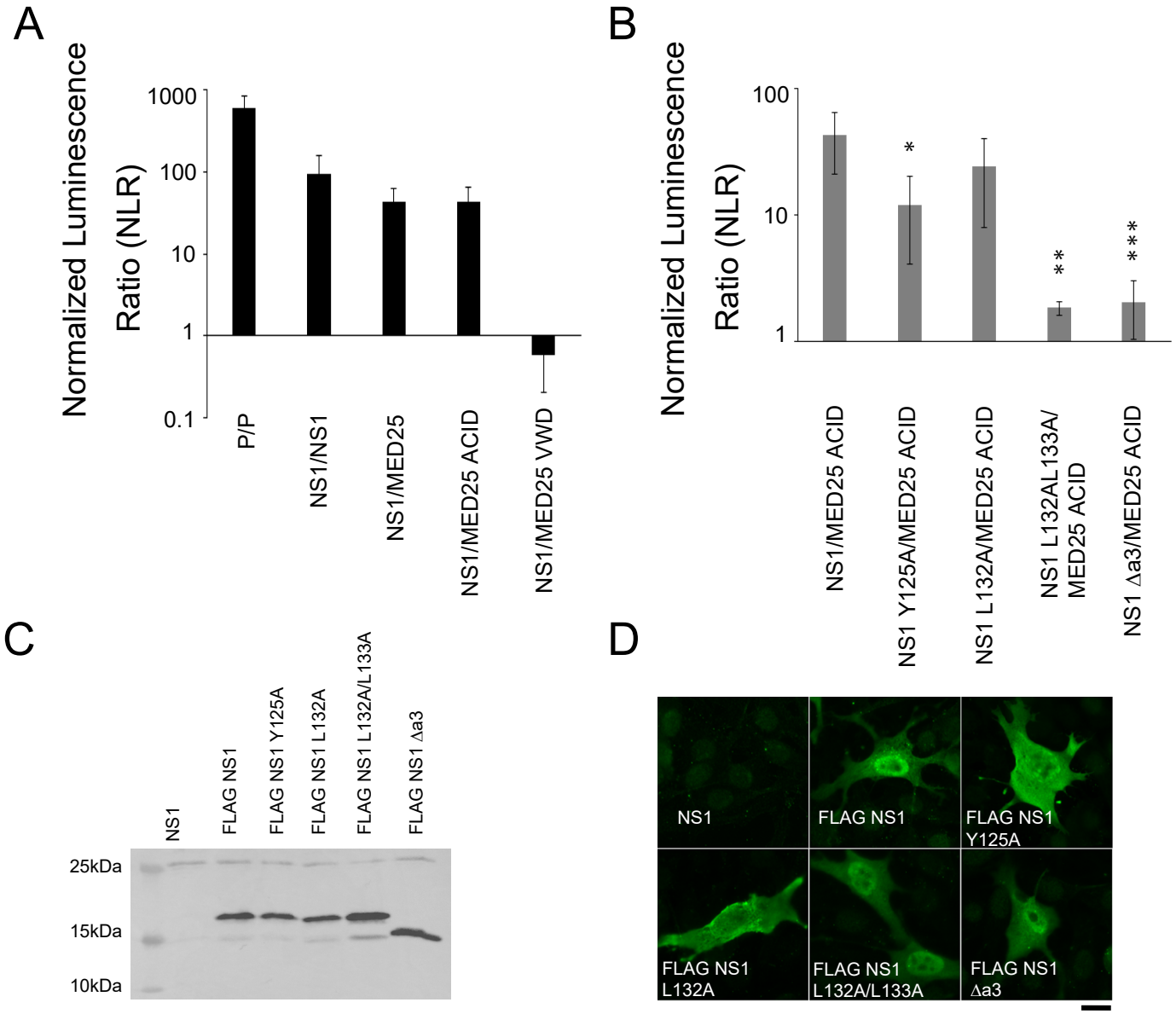

Fig. 3

A.

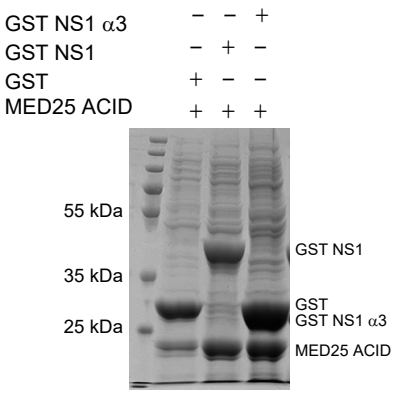

B.

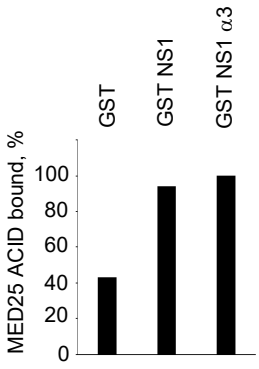

Fig. 4

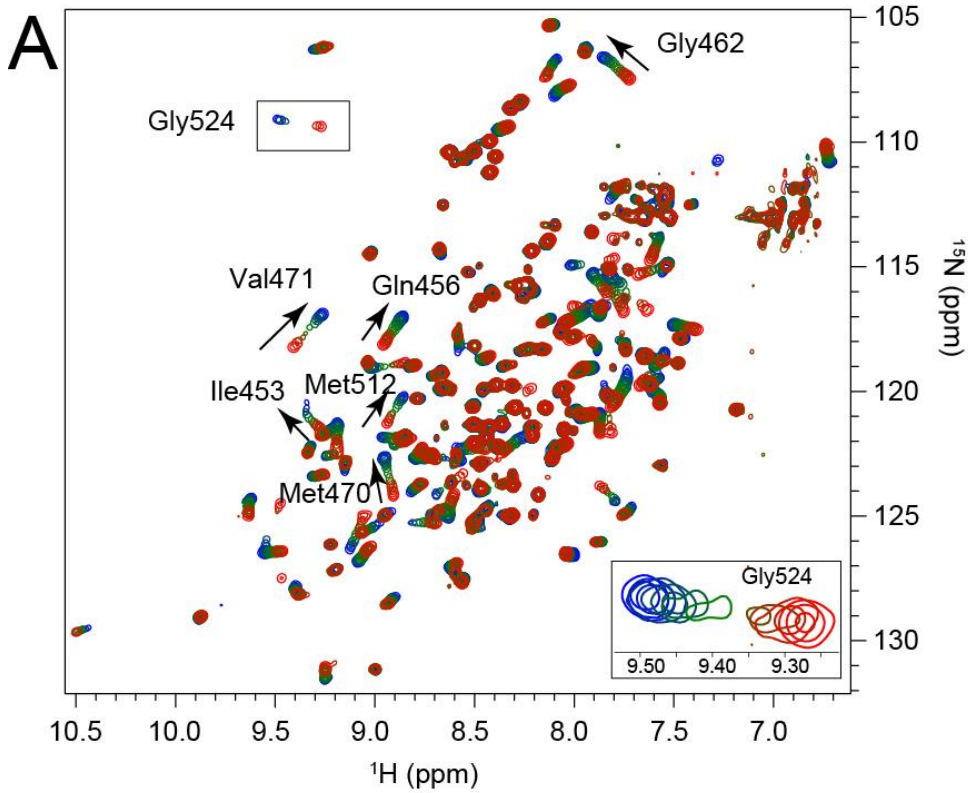
A
Gly462
Gly524
Val471
Gln456
Ile453
Met512
Met470
Gly524
9.50
9.40
9.30
105
110
115
120
125
130
15N (ppm)
10.5
10.0
9.5
9.0
8.5
8.0
7.5
7.0
1H (ppm)

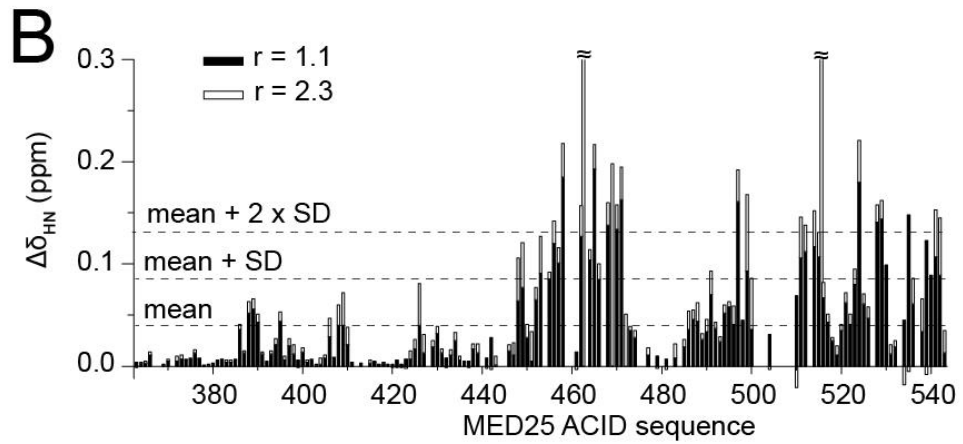
B
r = 1.1
r = 2.3
mean + 2 x SD
mean + SD
mean
0.3
0.2
0.1
0.0
ΔδHN (ppm)
380
400
420
440
460
480
500
520
540
MED25 ACID sequence

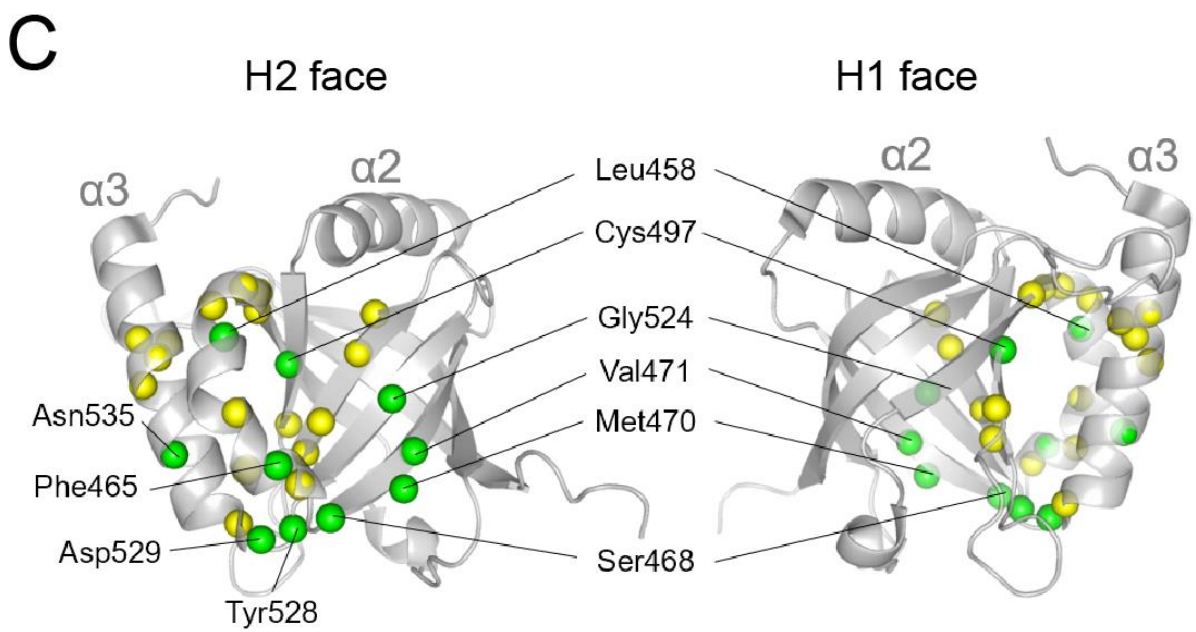
C
H2 face
H1 face
α3
α2
α2
α3
Leu458
Cys497
Gly524
Val471
Met470
Asn535
Phe465
Asp529
Tyr528
Ser468

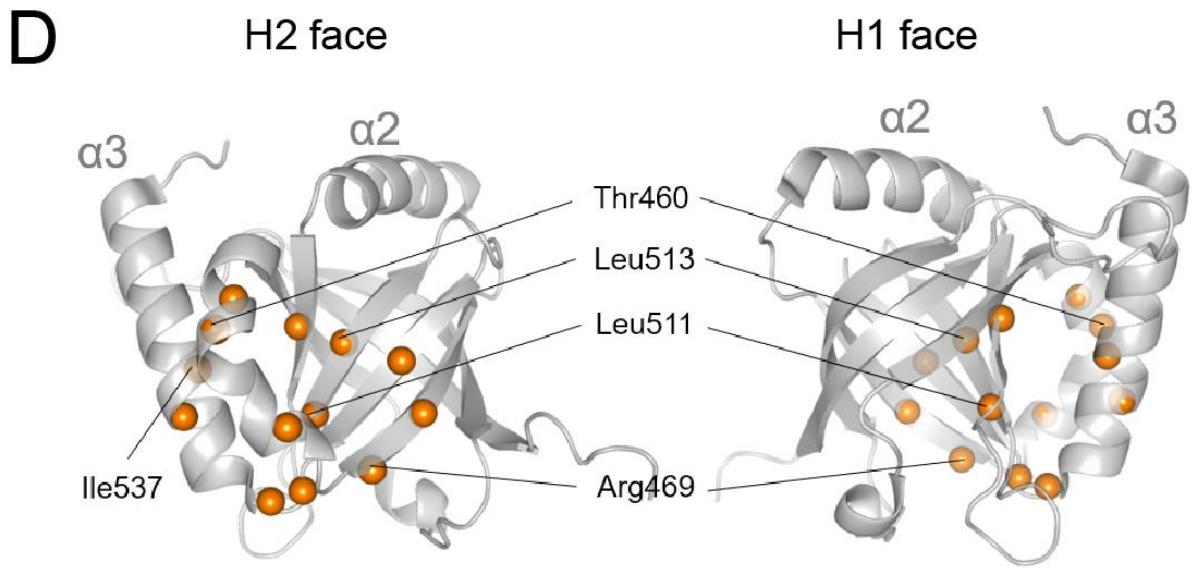
D
H2 face
H1 face
α3
α2
α2
α3
Thr460
Leu513
Leu511
Ile537
Arg469

Fig. 5

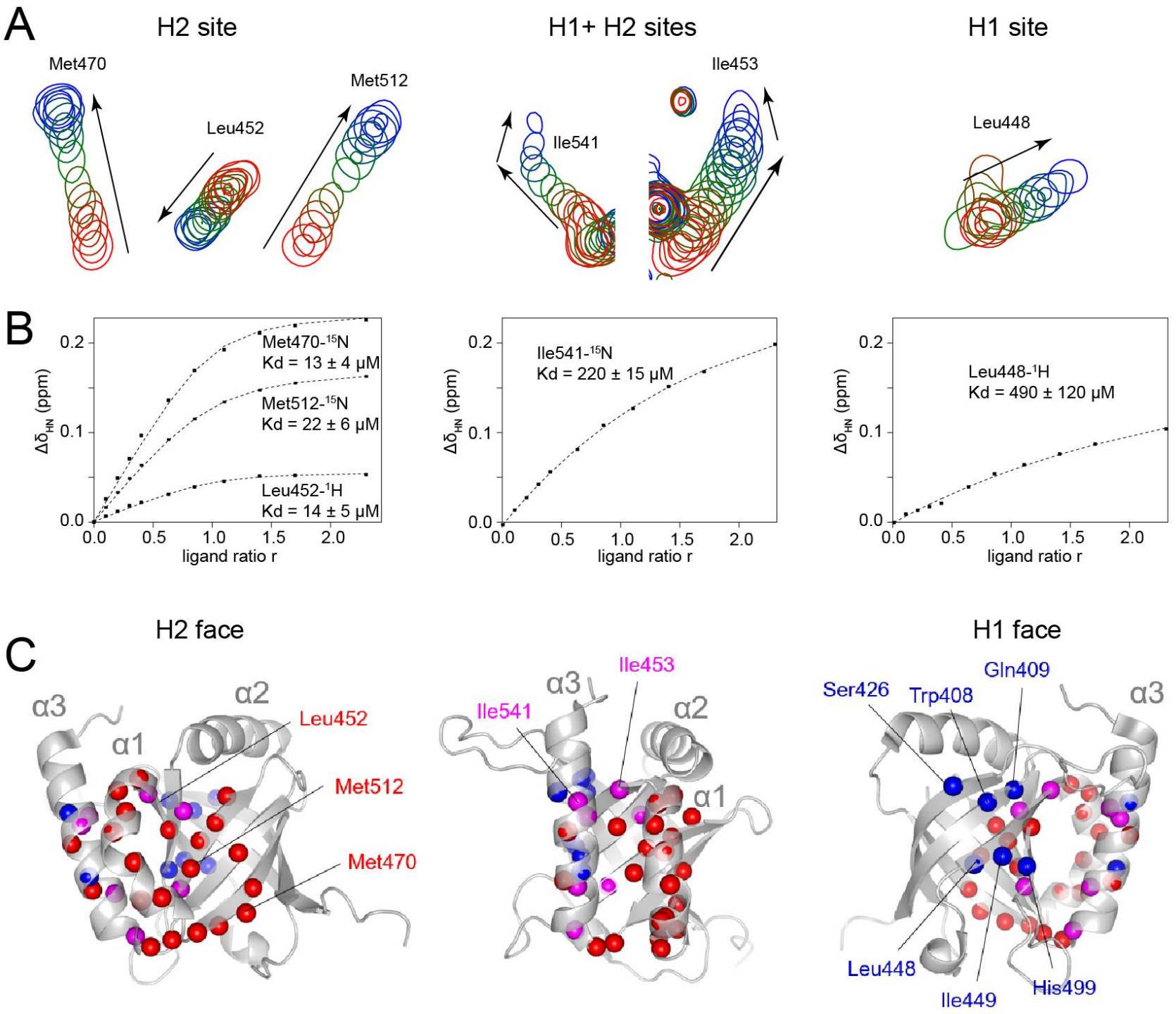
A
H2 site
H1+ H2 sites
H1 site
Met470
Met512
Leu452
Ile453
Ile541
Leu448
B
Met470-15N
Kd = 13 ± 4 μM
Met512-15N
Kd = 22 ± 6 μM
Leu452-1H
Kd = 14 ± 5 μM
Ile541-15N
Kd = 220 ± 15 μM
Leu448-1H
Kd = 490 ± 120 μM
ΔδHN (ppm)
ligand ratio r
C
H2 face
H1 face
α1
α2
α3
Leu452
Met512
Met470
Ile453
Ile541
Gln409
Ser426
Trp408
Leu448
Ile449
His499

Fig. 6

A.

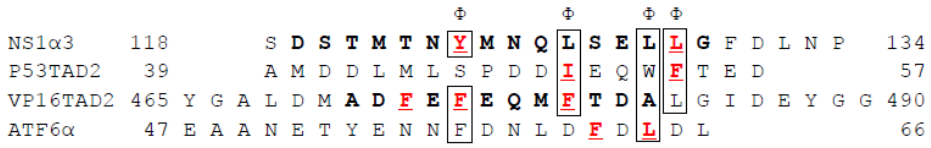

B.

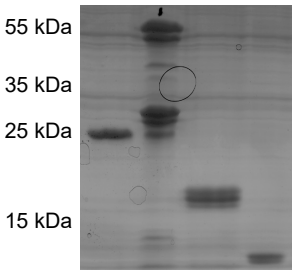

C.

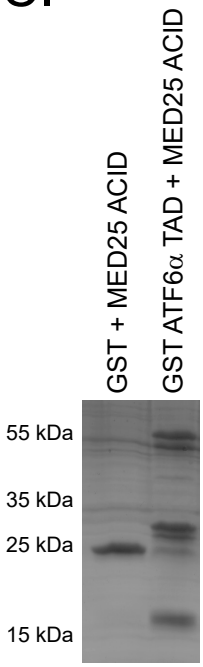

D.